ELSEVIER

Journal of Nuclear Materials 283–287 (2000) 329–333

journal of nuclear materials

www.elsevier.nl/locate/jnucmat

Microstructural changes induced by post-irradiation annealing of neutron-irradiated austenitic stainless steels

J.I. Cole *, T.R. Allen [1]

Argonne National Laboratory-West, P.O. Box 2528, Idaho Falls, ID 83403, USA

Abstract

Irradiated EBR-II hexagonal 'hex' duct material fabricated from 304 stainless steel (SS) is characterized prior to and following in situ annealing in the transmission electron microscope (TEM) at temperatures between 400°C and 600°C for various lengths of time. The hex duct samples were irradiated at temperatures between 375°C and 389°C to doses up to 29 dpa over a range of dose rates. The pre-annealed microstructure of the irradiated hex ducts exhibited substantial radiation-induced dislocation development (networks and loops) and cavity formation (bubbles and voids). Following annealing at all temperatures, dislocation loop densities decrease significantly and the dislocation network density increases. Annealing at 500°C and 600°C led to the shrinking or disappearance of many larger faceted voids. In addition to shrinkage of larger voids, small spherical bubbles formed leading to an increase in the overall cavity density and a decrease in the average cavity size.

1. Introduction

Formation of radiation-induced defect microstructures (cavities, dislocations, precipitates) can lead to dimensional changes, increase strength and promote embrittlement of reactor structural materials during service life. These issues will be even more critical for fusion reactor components due to high rates of atomic displacement and generation of transmutation-induced helium. Mitigation of radiation damage effects through moderate temperature annealing (0.3–0.5 the melting temperature) is one possible method of recovering properties of structural materials [1,2]. The thermal stability of the radiation-induced defect structures, as well as the kinetics of damage recovery will dictate the practicality of this approach. However, experimental data on the impact of moderate temperature annealing on radiation-induced microstructures are lacking.

In order to investigate the long-term effects of neutron irradiation on structural materials, a substantial number of components from the experimental breeder reactor EBR-II were recovered during final shutdown operations. The majority of these materials are in the form of austenitic stainless steel (SS) hexagonal ducts used to house the reactor subassemblies (fuel, reflectors, experiments, etc.). Due to the gradients in fluence, flux and temperature as a function of core location, these hex ducts underwent a variety of irradiation conditions both axially (along the length of the duct), and radially (extending out from the core center) and provide a significant opportunity for studying the impact of long-term low dose rate irradiation on alloys widely used in nuclear power systems.

For the current study, observations were made on the microstructures of irradiated 304 SS hexagonal duct material, which has been irradiated to different doses in the temperature range 375–389°C producing a range of irradiation-induced void and dislocation structures. Changes in the microstructure are examined at annealing temperatures between 400°C and 600°C and for times up to 4 h.

2. Experimental

The composition of the 304 hexagonal duct material examined is given in Table 1, while Table 2 provides the

* Corresponding author. Tel.: +1-208 533 7165; fax: +1-208 533 7863.

E-mail addresses: jim.cole@anlw.anl.gov (J.I. Cole), todd.allen@anlw.anl.gov (T.R. Allen).

[1] Tel.: +1-208 533 7760; fax: +1-208 533 7863.

0022-3115/00/$ - see front matter
PII: S0022-3115(00)00072-6

Table 1
Composition of EBR-II 304 stainless steel hex duct

Cr	Ni	Mn	Si	Mo	C	Fe
18.6	9.1	0.80	0.46	<0.036	892 wppm	Balance

dose, dose rate and irradiation temperatures for the four samples examined. The starting condition of the hex ducts was mill annealed. Two of the hex ducts which were irradiated to a similar dose of 10 and 12 dpa, respectively (samples B and C) underwent a different irradiation history. While hex duct C was left in the same position throughout its lifetime, hex duct B was moved to a position further away from the core centerline, where it experienced a substantially lower dose rate. Differences in irradiation history produced different irradiation-induced microstructures as discussed in an earlier study [3]. Analysis was carried out in the trans-

Table 2
Irradiation parameters

Hex duct designation	Temperature (°C)	Dose (dpa)	Average dose rate (dpa/s)
A	387	29.9	1.1×10^{-7}
B	375	10.6	4.6×10^{-8}
C	378	12.2	4.7×10^{-8}
D	388	26.0	1.0×10^{-7}

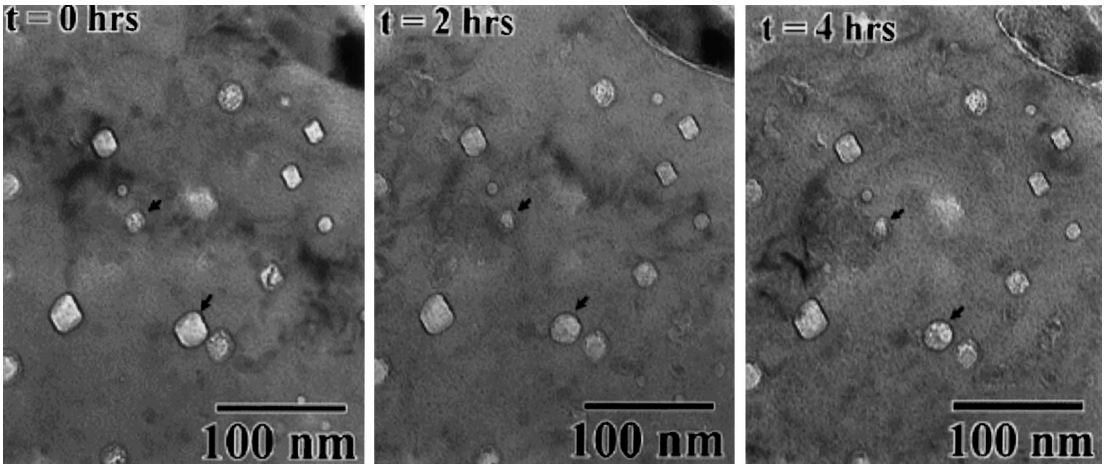

Fig. 1. Void microstructures in the 304 SS hex duct samples as a function of annealing time at 400°C. Arrows delineate voids which have become more spherical upon annealing.

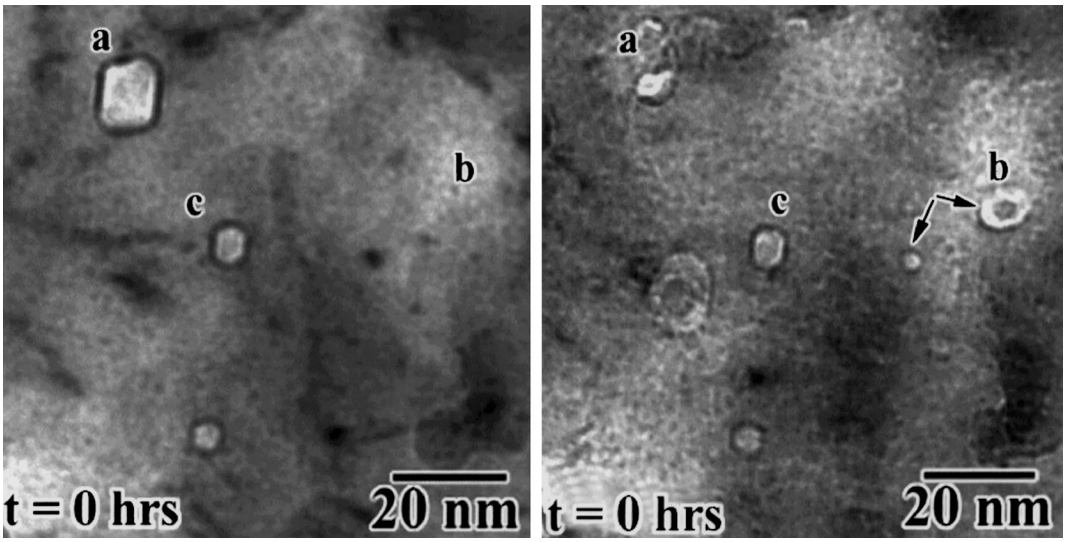

Fig. 2. Higher magnification images of hex duct C at 0 and 4 h of annealing: (a) the shrinkage of a faceted void; (b) the formation of a bubble in association with a precipitate and (c) the absence of change in an existing cavity.

mission electron microscope (TEM) at an accelerating voltage of 200 kV. In situ annealing experiments were conducted using a double tilt heating stage. The samples were annealed for periods of 2 and 4 h and examined after each time period.

3. Results

Hex duct A (irradiated to 29 dpa) exhibited a high density of larger cavities. The faceted geometry of these cavities indicates they are voids. There was no significant difference in void density upon annealing at 400°C for up to 4 h, however, a few of the larger faceted voids shrank and became more spherical (Fig. 1).

Hex ducts B and C were both annealed at 500°C to evaluate if a difference in initial void microstructure had an impact on annealing behavior. As mentioned earlier, two types of void microstructures existed in B and C although they had been irradiated to similar dose levels (~11 dpa). Sample B had a lower density of small cavities (<10 nm) and C had a higher density of larger cavities. The cavities consisted of a combination of small bubbles and larger voids.

TEM analysis of ducts B and C revealed that at 500°C several of the larger faceted voids had shrunk substantially or disappeared completely upon annealing. However, this did not occur with all of the voids, as many of them remained unchanged. Frequently, the unchanged voids had similar geometry and surroundings to voids that had disappeared. Accompanying the disappearance of the larger faceted voids, the formation of small (1–5 nm) bubbles occurred. Many of these bubbles are associated with small second phase precipitates. Due to their small size, these precipitates could not be identified. Fig. 2, which shows higher magnification images of hex duct C at 0 and 4 h of annealing, illustrates (a) the shrinkage of a faceted void, (b) the formation of a bubble around a small precipitate, and (c) the absence of change in many of the existing cavities. The bubble density increases with annealing time from 2 to 4 h.

Annealing of hex duct D at 600°C (irradiated to 26 dpa) exhibits similar behavior to the hex ducts annealed at 500°C. Pre-annealed voids sizes and densities in this hex duct were greater than duct B and C due to the higher dose. As with the hex ducts annealed at 500°C, many of the larger faceted voids shrink or disappear, while smaller bubbles form. The main difference between the annealing behavior at 500°C and 600°C is that the minimum bubble size in the hex duct annealed at 600°C is larger (closer to 5 nm).

Plots of average cavity diameter and density as a function of annealing time are provided in Fig. 3 for the hex ducts annealed at 500°C and 600°C. The plots show that within the first 2 h of annealing, the overall cavity density increases and the average void diameter decreases. The decrease in average cavity diameter and increase in density result from the formation of the high density of small bubbles. The density increase for hex duct C, which initially had a lower density of cavities, which were smaller, was substantially greater than in sample B annealed at the same temperature. The increase in void density for hex duct D, annealed at 600°C, behaved similarly to hex duct C. In two of the hex ducts (B and D), the average void diameter appears to either have leveled off (D) or be increasing (B).

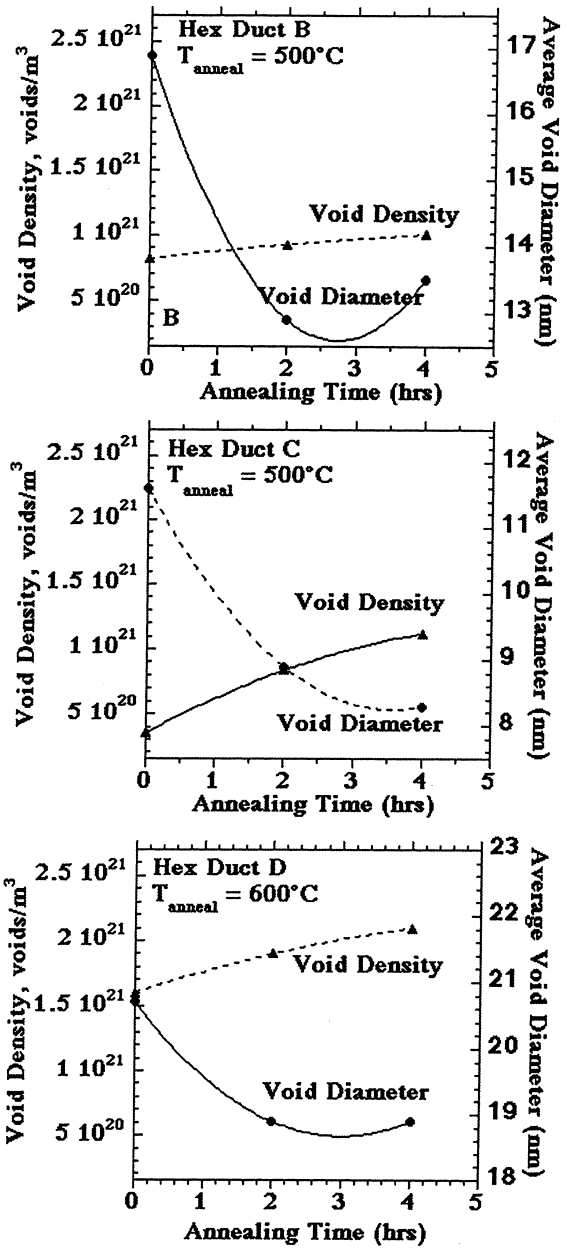

Fig. 3. Plots of cavity density and diameter as a function of annealing time.

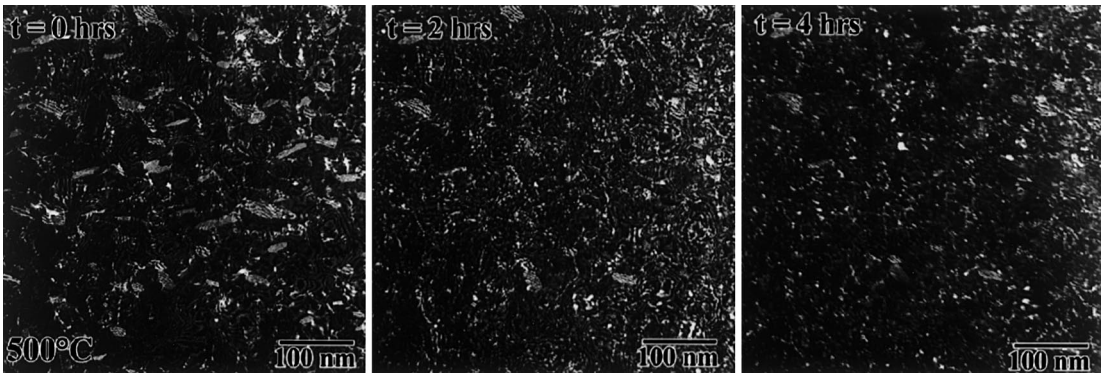

Fig. 4. WBDF images of dislocation microstructure in hex duct A as a function of annealing time.

Dislocation loop density decreases substantially after 2 h of annealing at all of the temperatures examined. Weak beam darkfield (WBDF) micrographs of the loops in sample A as a function of annealing time are provided in Fig. 4. Loops appear to unfault and form a dense dislocation network. Further annealing to 4 h results in a moderate decrease in the network dislocation density, and a reduction in the faulted loop density. Due to the nature of the TEM thin foil, it is quite possible that once loops unfault and become mobile on the slip plane, they will glide to the surface due to image forces and be eliminated. As a result, the density of dislocations in the thin foil should be less than in bulk samples.

4. Discussion

Formation of small bubbles following annealing was not observed in several other studies [4–6] and substantial void shrinkage did not occur until higher annealing temperatures (>700°C). This may be due to the shorter annealing times used in these studies (only 1 h at all temperatures). Calculations in these earlier studies also reveal that upon annealing, the larger voids shrink to the point were the total void volume is comparable to the amount of transmutation-induced He [4].

Small bubble nucleation has been observed in irradiated steels with high helium generation rates at lower irradiation temperatures [7]. It is quite likely that there are many existing He atom clusters prior to annealing, which are too small to observe in the TEM. Upon annealing the He bubbles act as traps for vacancies and thus grow to a size observable in the TEM. As the plots for average cavity size as a function of annealing time suggest (Fig. 3), the bubbles may continue to grow with annealing time as more vacancies are captured. Eventually, some equilibrium size will be reached.

Comparing these results to that of Holmes et al. [5], reveals that in their study, there was not a reduction in dislocation loop size during annealing for 1 h at 480°C, while in this study loops disappeared after annealing for 2 h at 400°C. As suggested earlier, the reason for the dramatic decrease in loop density upon annealing at all temperatures may be due to loop unfaulting and gliding to the foil surface. An additional study conducted by Busby [2] indicates that small black spot loops formed by irradiating at lower temperature are stable (loop density remains unchanged) after 1 h of annealing at 500°C. Further studies will have to be performed to compare differences between annealing behavior in bulk samples compared to in situ studies with thin foils.

Consequences of the observed microstructural changes to alloy properties may be significant. Because large voids and faulted dislocation loops are the strongest barriers to plastic deformation [8], a reduction in their density should improve alloy ductility. Tensile tests on irradiated and annealed 304 SS [4] indicate that this is true. The impact the formation of a large density of small bubbles has on mechanical properties is unclear. However, studies suggest [8] that these small bubbles are much less effective strengtheners than the larger voids.

5. Conclusions

In situ annealing of 304 SS hexagonal duct material retrieved from EBR-II indicates that there is a dramatic reduction in faulted dislocation loop density during annealing at temperatures between 400°C and 600°C. With respect to the cavity structure, annealing at temperatures between 500°C and 600°C leads to the shrinkage or disappearance of many of the larger faceted voids, and the formation of small (1–5 nm) He bubbles.

Acknowledgements

Work supported under contract W-31-109-Eng-38 with the US Department of Energy.

References

[1] A.J. Jacobs, S. Dumbill, in: Proceedings of the Seventh International Symposium on Environmental Degradation of Materials in Nuclear Power Systems – Water Reactors, NACE International, Houston, TX, 1995, p. 1021.
[2] J.T. Busby, G.S. Was, E.A. Kenik, in: S.J. Zinkle, G.E. Lucas, R.C. Ewing, J.S. Williams (Eds.), Microstructural processes in irradiated materials, vol. 540, Materials Research Society, Boston, MA, 1999, p. 495.
[3] J.I. Cole, T.R. Allen, in: S.J. Zinkle, G.E. Lucas, R.C. Ewing, J.S. Williams (Eds.), Microstructural Processes in Irradiated Materials, vol. 540, Materials Research Society, Boston, MA, 1999, p. 495.
[4] D.L. Porter, G.L. McVay, L.C. Walters, in: D. Kramer, H.R. Brager, J.S. Perrin (Eds.), Effects of Radiation on Materials: Tenth Conference, ASTM STP 725, American Society for Testing and Materials, 1981, p. 500.
[5] J.J. Holmes, R.E. Robbins, J.L. Brimhall, B. Mastel, Acta Metall. 16 (1968) 955.
[6] J.O. Stiegler, E.E. Bloom, J. Nucl. Mater. 33 (1969) 173.
[7] L.E. Thomas, J.M. Beeston, J. Nucl. Mater. 107 (1982) 159.
[8] G.E. Lucas, J. Nucl. Mater. 206 (1993) 287.